Supporting Information

McConnell Smith et al. 10.1073/pnas.0810588106

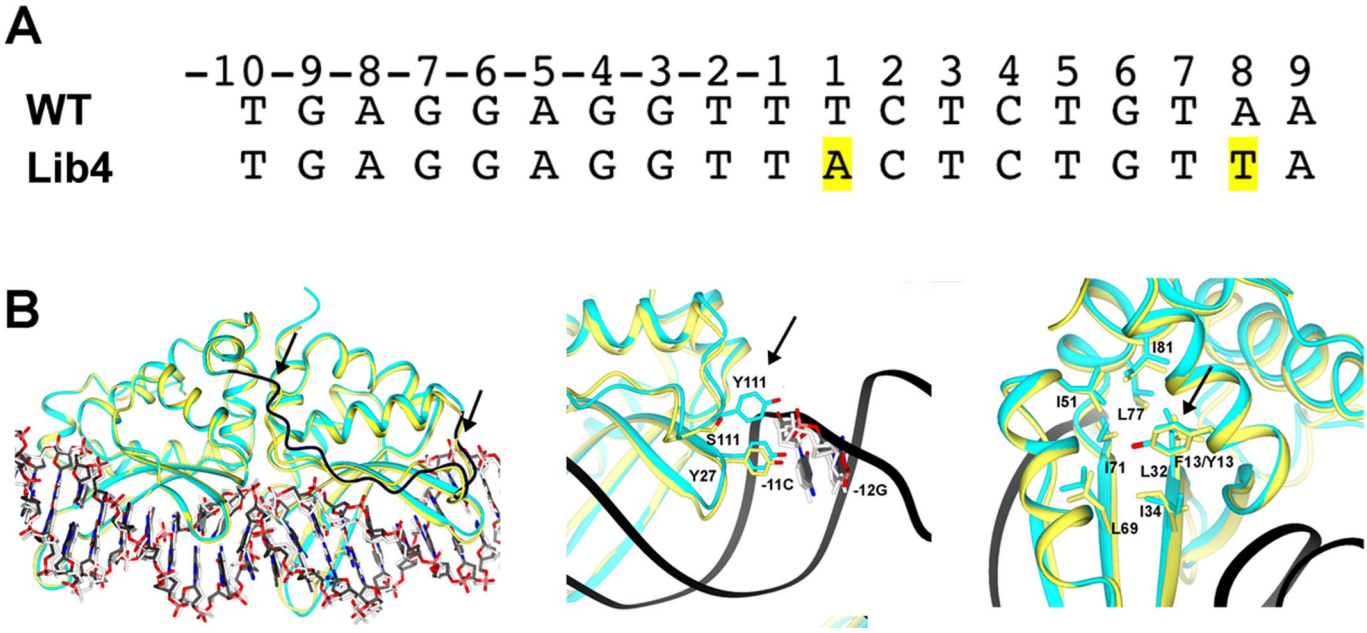

Fig. S1. Variant enzyme scaffolds and target sites used in this study. (*A*) The wild-type I-AniI target site corresponds to a 19-bp coding sequence in the mitochondrial cytochrome *b* oxidase gene in the host organism *Aspergillus nidulans*. The Lib4 target site was identified in an in vitro screen for cleavable target site variants [Scalley-Kim M, McConnell-Smith A, Stoddard BL (2007) Coevolution of a homing endonuclease and its host target sequence. *J Mol Biol* 372:1305–1319]. This sequence contains two base pair substitutions (highlighted above) that increase in vitro binding affinity and cleavage by native I-AniI by ≈5-fold. (*B*) The Y2 endonuclease scaffold of I-AniI (cyan), differs from the native scaffold (yellow) at two residues, where F13Y and S111Y substitutions (see arrows above) increase DNA binding affinity and improve catalytic activity at physiological (30–37 °C) temperatures. Native I-AniI binds its target site with a dissociation constant (K_d) of ≈90 nM and exhibits a temperature optimum of ≈55 °C, whereas Y2 I-AniI binds native target site DNA with a K_d of ≈10 nM and a temperature optimum of ≈35 °C. The Y2 construct was identified in an in vivo screen for enzyme variants that exhibit improved cleavage of native I-AniI target site DNA at 30 °C [Takeuchi R, Certo M, Caprara MG, Scharenberg AM, Stoddard, BL (December 2008) Optimization of in vivo activity of a bifunctional homing endonuclease and maturase reverses evolutionary degradation. *Nucleic Acids Res*, 10.1093/nar/gkn1007.]

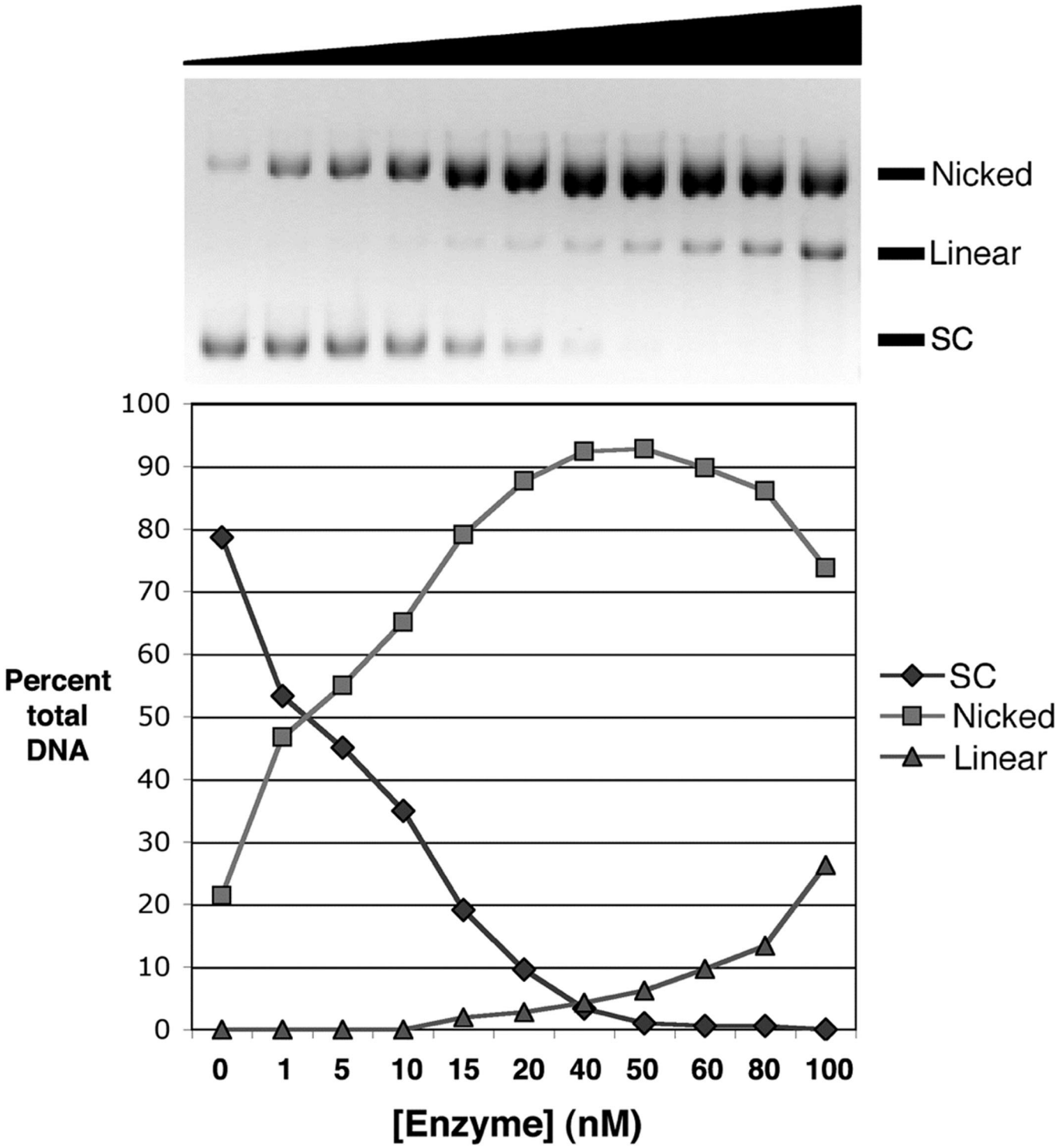

Fig. S2. DNA nicking and cleavage activity of Y2 I-AniI nickase. (*Upper*) Digests of supercoiled substrate plasmid with increasing concentrations of I-AniI Y2 nickase. Digests were for 2 h using 10 nM DNA plasmid substrate and I-AniI Y2 nickase protein ranging from 1 to 100 nM under digest conditions described in *Methods*. (*Lower*) Quantitation of gel data shown in *Upper*. Longer digests at 1–10 nM enzyme (≤1:1 molar ratio) did not generate detectable linearized product.

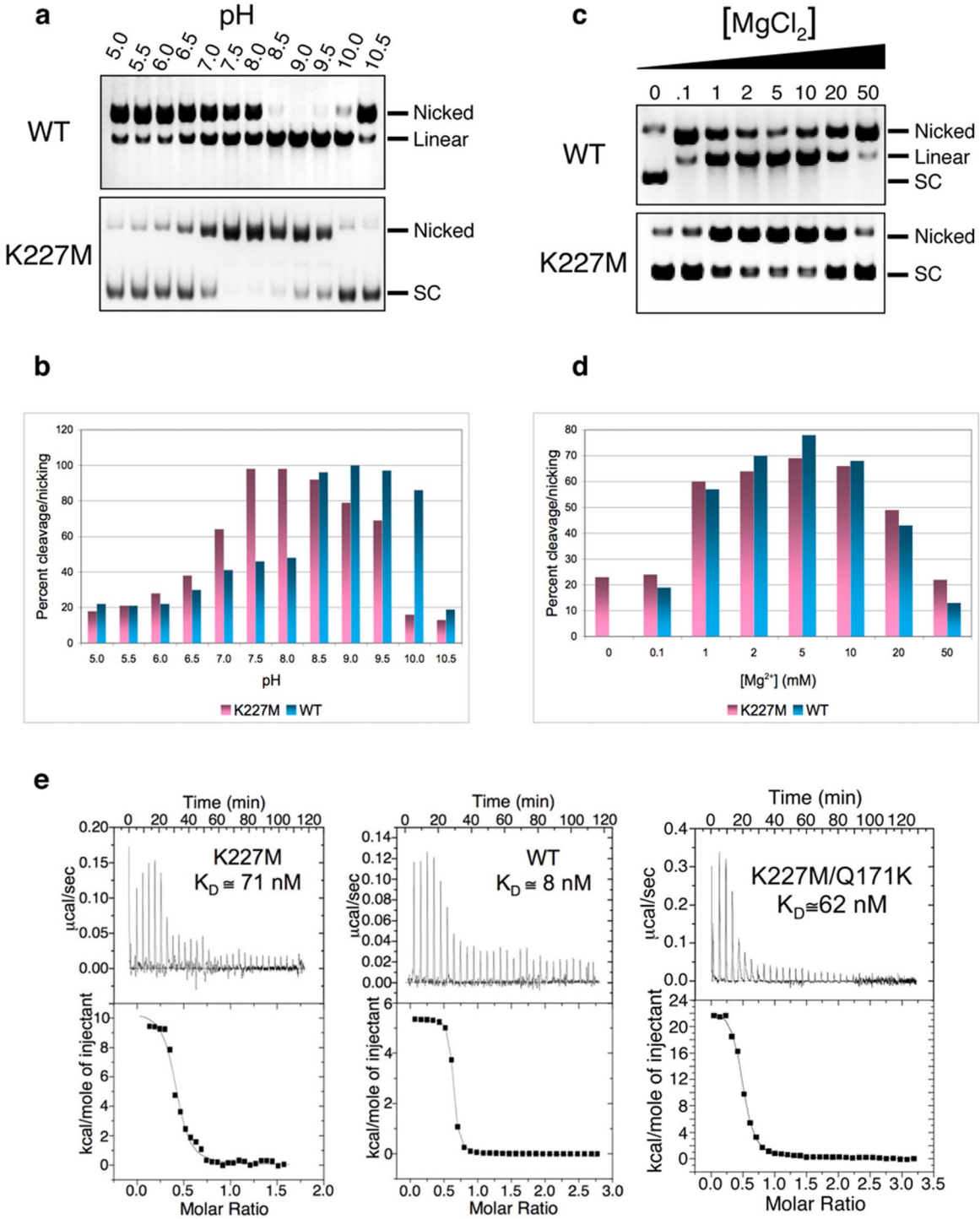

Fig. S3. (*a*) pH profile. Supercoiled substrate plasmid was digested with 0.5–1 μM wile-type (WT) or K227M I-AniI at the specified pH, and reactions were stopped before reaching completion. (*b*) Percentage cleavage or nicking vs. pH for both enzymes. Gel bands were quantified with ImageJ. Intensities of nicked, linearized, and supercoiled plasmid were compared in each lane to determine the percentage cleavage. (*c*) Metal dependence profile. Supercoiled substrate plasmid was digested as in *a* at the specified $MgCl_2$ concentration (in mM). (*d*) Percentage cleavage or nicking vs. magnesium concentration for WT and nicking I-AniI. Quantification was as in *b*. (*e*) Relative binding of dsDNA substrate by I-AniI K227M nickase, WT I-AniI, and catalytically inactive K227M/Q171K I-AniI variant as measured by isothermal titration calorimetry [Eastberg JH, *et al*. (2007) Thermodynamics of DNA target site recognition by homing endonucleases. *Nucleic Acids Res* 35:7209–7221]. K_d values are averages of three independent experiments. Although the estimated molar ratios of binding for experiments shown in these panels are slightly below 1:1, the average of multiple runs in each case indicates a 1:1 binding stoichiometry of protein to DNA duplex.

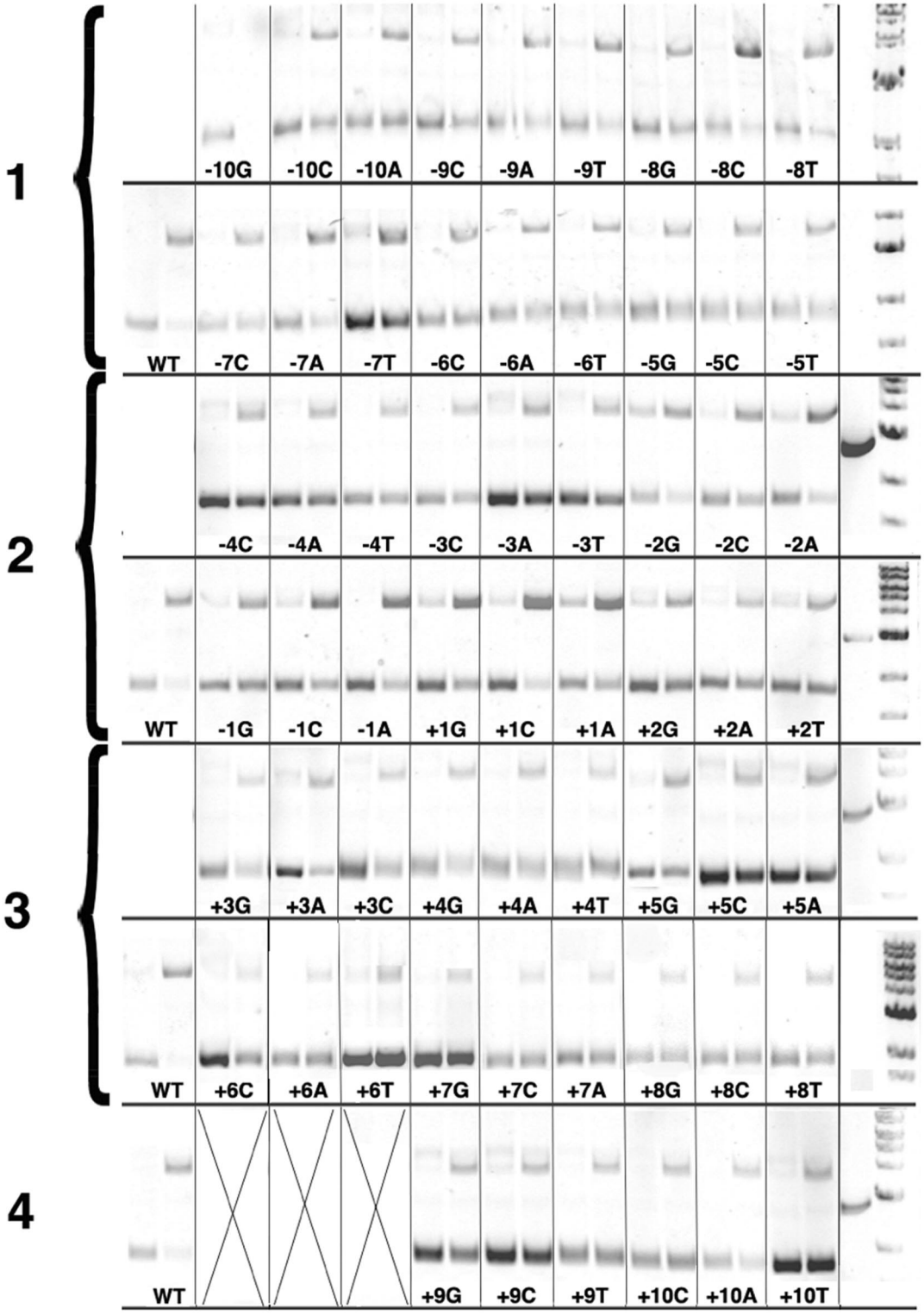

Fig. S4. I-AniI nickase cleavage of target sites with 1-bp substitutions. A target site matrix consisting of 60 separate base substitutions was used to determine the ability of I-AniI nickase to cleave mutant target sites. A single preparation of I-AniI nickase protein was used to generate the cleavage results shown above. Digests were performed over a period of 4 days (day numbers shown at left). On each day, a standard series of digests using a native I-AniI target site was performed to control for loss or change in the enzyme's specific activity; none was detected. These control digests are shown in the far left column (WT). The remaining panels contain pairs of lanes representing a no-enzyme control (left) and digest products (right) of the indicated single base-substituted target site. The rightmost column includes a DNA molecular mass control corresponding to linearized plasmid, followed by a marker DNA ladder. Cleavage experiments were performed three times, and the averaged extent of cleavage for each substrate was used to construct the relative cleavage sensitivity plot shown in Fig. 3.

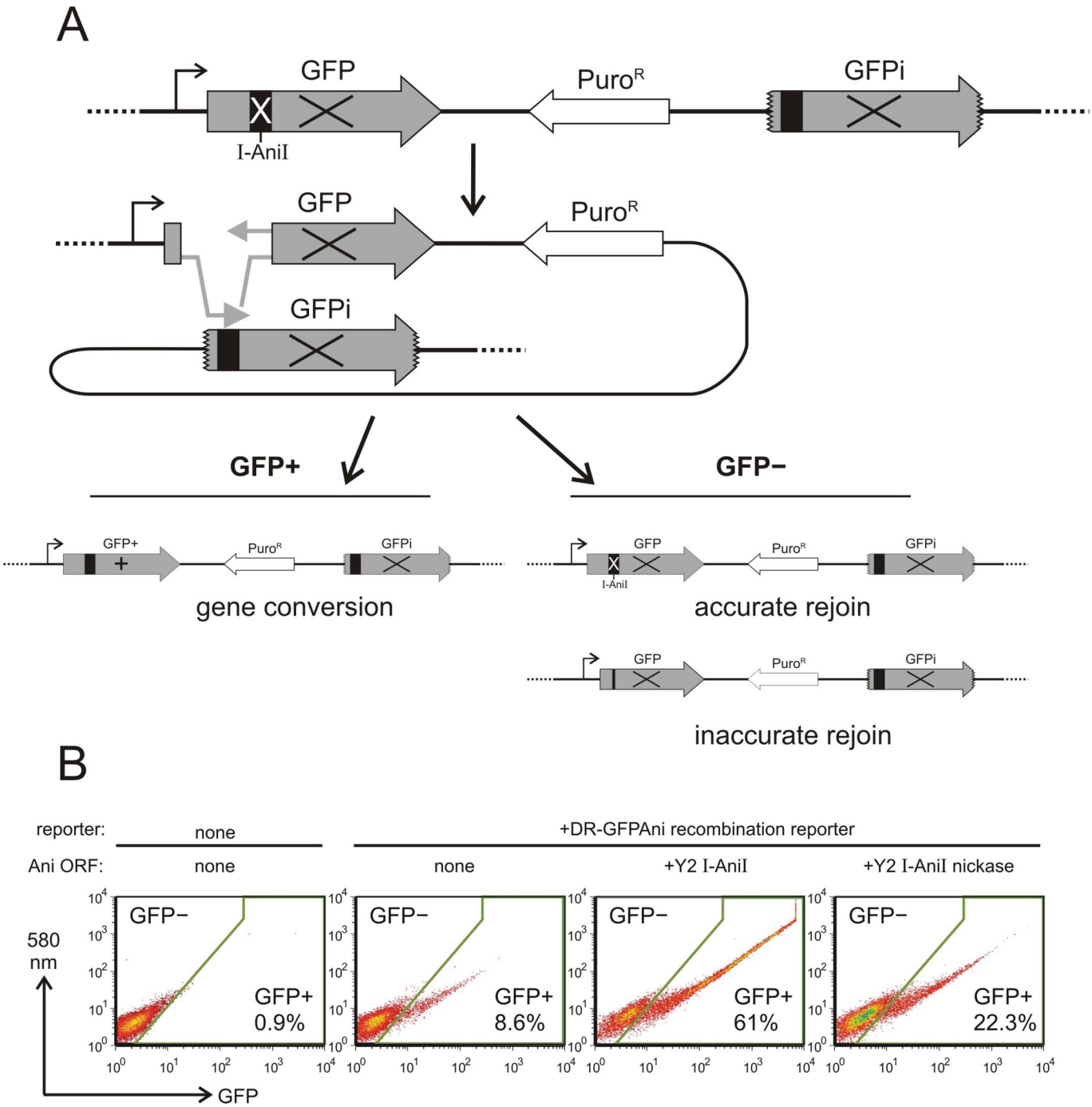

Fig. S5. Plasmid-based gene conversion *in cis* in human cells. (*A*) The DR-GFPAni reporter [Pierce AJ, Johnson RD, Thompson LH, Jasin M (1999) XRCC3 promotes homology-directed repair of DNA damage in mammalian cells. *Genes Dev* 13:2633–2638] consists of two nonfunctional GFP genes (dark gray arrows, top row). The upstream GFP gene is interrupted by an I-AniI site and a stop codon (black box with the white X). The homologous sequence in the downstream copy is truncated on both 5′ and 3′ ends. Generation of a double-strand break (DSB) or nick by I-AniI in the upstream GFP gene triggers repair using the downstream truncated copy of GFP as a repair template to generate a functional GFP copy (GFP^+, lower left) by gene conversion. These GFP^+ events are detected and quantified by flow cytometry. Alternatively, DSB or nick ends can be rejoined (GFP^-, lower right). Accurate rejoining restores the I-AniI site, whereas inaccurate repair after end resection or addition generates an I-AniI-resistant, GFP-mutant allele. (*B*) Examples of flow output of 293T cells transfected with the DR-GFPAni reporter shown in *a*, and either no expression plasmid or an expression vector for Y2 I-AniI cleavase or nickase protein as described in *Methods*. (*Left two frames*) Background autofluorescence of the cell line after mock transfection, or transfection with the DR-GFPAni reporter plasmid. (*Right two frames*) Fluorescence-activated cell sorting profiles of cells cotransfected with the pDR-GFPAni reporter plasmid and either a Y2 I-AniI Y2 cleavase or Y2 I-AniI nickase expression vector. The percentage of GFP^+ cells is shown in the lower right in each panel. Transfection efficiency in all experiments was >90% as assessed by transfection of a control pEGFP-C1 coding plasmid (Clontech).

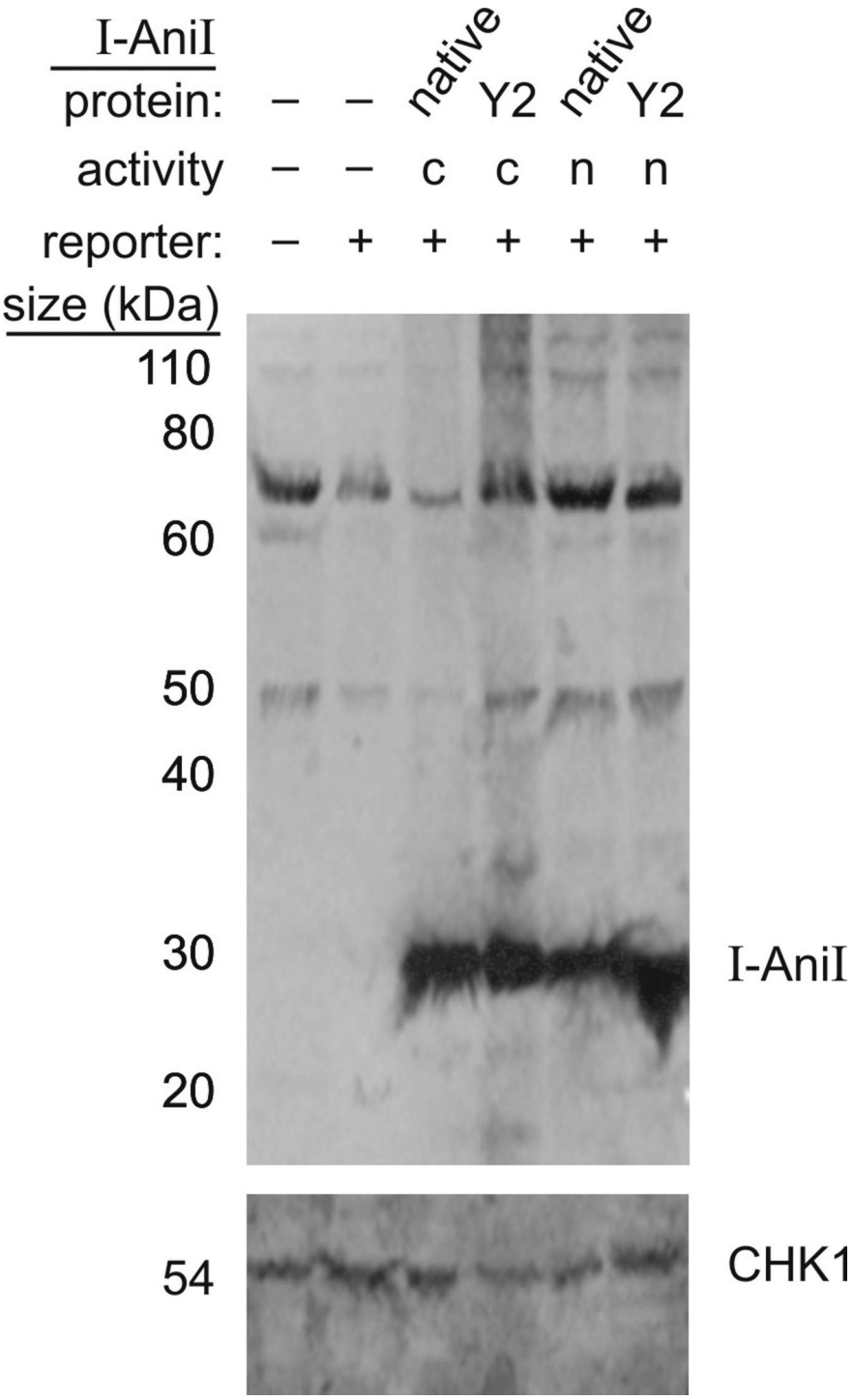

Fig. S6. Expression levels of I-AniI variants transfected into 293T human cells. Western blot analysis was used to confirm and estimate the level of expression of I-AniI proteins in vivo. I-AniI and Y2 I-AniI cleavase (c, cleavase) or nickase (n, nickase) proteins were expressed by transient transfection of human 293T cells. Cellular extracts were prepared from transfected cells used for GFP^+ recombination analyses shown in Fig. S5. Experimental details: cell pellets from ≈50,000 cells transfected with each indicated I-AniI expression vector were lysed 48 h after transfection in buffer [25 mM Tris·HCl (pH 8.0), 5 mM EDTA, 0.6 M NaCl, 10% (vol/vol) glycerol, 0.01 mM DTT, 0.1% Nonidet P-40, protease inhibitor] for 40 min on ice. Total protein amount was estimated by Bradford assay, and 2 μg of total protein from each sample separated on a 4–12% NuPAGE Bistris gradient gel (Invitrogen). Proteins were then transferred onto PVDF membrane (Osmonics) for immunodetection using a mouse-α-HA primary antibody (1.583.816; Roche) at a 1:2,000 dilution followed by detection with a goat-α-mouse IgG(H+L)/horseradish peroxidase (HRP)-conjugated secondary antibody (1031-05; Southern Biotech). The loading control protein CHK1 was detected after stripping the membrane and reprobing with a mouse-α-Chk1 (SC-8404; Santa Cruz Biotechnology) primary antibody and a goat-α-mouse IgG(H+L)/HRP (1031-05; Southern Biotech). Blot images were captured using ECL Plus (GE Healthcare) together with imaging on a STORM 840 PhosphorImager (GE Healthcare).

Table S1. Frequency of GFP$^+$/plasmid/in *cis*-targeted recombination experiments

Reporter/target site	Endonuclease*	No. of experiments	Mean GFP$^+$, %	±SD, %
Series 1†				
None (cells alone)	None	3	0.20	0.10
EGFP-C1 (positive control)	None	3	91.83	2.19
pDRGFP/native	None	3	5.10	2.21
pDRGFPLib4	None	3	5.93	1.70
pDRGFP/native	I-AniI	3	11.03	0.58
pDRGFP/Lib4	I-AniI	3	10.37	3.23
pDRGFP/native	Y2 I-AniI	3	47.47	2.29
pDRGFP/Lib4	Y2 I-AniI	3	32.23	1.54
pDRGFP/native	I-AniI nickase	3	2.93	0.15
pDRGFP/Lib4	I-AniI nickase	3	2.97	1.96
pDRGFP/native	Y2 I-AniI nickase	3	12.40	1.85
pDRGFP/Lib4	Y2 I-AniI nickase	3	9.40	1.51
Series 2†				
None (cells alone)	None	3	0.77	0.51
EGFP-C1 (positive control)	None	3	98.93	0.21
pDRGFP/native	None	3	11.50	2.54
PDRGFP/native	I-AniI	3	20.00	3.73
pDRGFP/native	Y2 I-AniI	3	58.40	3.99
pDRGFP/native	I-AniI nickase	3	3.83	1.53
pDRGFP/native	Y2 I-AniI nickase	3	20.13	1.89
pDRGFP/native site Mutant	Y2 I-AniI nickase dead	3	15.10	2.51

The two different series were performed as described in *Methods*. The *cis* Series 1 assays were performed with propidium iodide counterstaining prior to flow cytometry, whereas Series 2 did not include this additional staining step. Series 2 data for are plotted in Fig. 4.

*The I-AniI endonuclease proteins used were: I-AniI HyperK (I-AniI), containing a silent G25G mutation to disrupt a cryptic splice site together with F80K and L232K substitutions; the Y2 variant of I-AniI, that includes F13Y and S111Y substitutions [Takeuchi R, et al. (December 2008) Optimization of in vivo activity of a bifunctional homing endonuclease and maturase reverses evolutionary degradation. *Nucleic Acids Res*, 10.1093/nar/gkn1007]; and a catalytically inactive dead mutant of Y2 I-AniI nickase that includes an additional active-site Q171K substitution in addition to the nickase K227M substitution (see *Results*).

Table S2. Frequency of GFP/integrated in *trans* recombination experiments

Reporter*	Donor*	Endonuclease†	No. of experiments	Mean GFP$^+$, %	±SD, %
Series 1					
pZF-GFPAni	GFPt	None	3	0.0020	0.00081
pZF-GFPAni	None	Y2 I-AniI	4	0.0019	0.00072
pZF-GFPAni	None	Y2 I-AniI nickase	4	0.0022	0.0015
pZF-GFPAni	GFPt	Y2 I-AniI	4	0.059	0.024
pZF-GFPAni	GFPt	Y2 I-AniI nickase	4	0.016	0.0032
Series 2					
pZF-GFPAni	GFPt	None	2	0.0014	0.000041
pZF-GFPAni	None	Y2 I-AniI	2	0.0016	0.00033
pZF-GFPAni	None	Y2 I-AniI nickase	2	0.0016	0.00022
PZF-GFPAni	GFPt	Y2 I-AniI	2	0.048	0.018
pZF-GFPAni	GFPt	Y2 I-AniI nickase	2	0.012	0.0037
pZF-GFPAni	None	Y2 I-AniI nickase dead mutant	2	0.0016	0.00031
pZF-GFPAni	GFPt	Y2 I-AniI nickase dead mutant	2	0.0021	0.00094

The two different series were performed as described in *Methods*. Series 2 data are plotted in Fig. 4.

*The integrated reporter plasmid pZF-GFPAni consists of the 5′ end of the pDR-GFPAni containing an I-AniI Lib4 target site and an adjacent 4 kb poly-lacO array inserted downstream of the GFP cassette [Cummings WJ, et al. (2007) Chromatin structure reglates gene conversion. *PLoS Biol* 5:e246]. A clonally derived 293T subline containing the chromosomally integrated reporter was used as a repair target, and a truncated 3′ GFP cassette from pDR-GFPAni as a transfected repair template (GFPt) in *trans* recombination experiments.

†The I-AniI endonuclease proteins used were: I-AniI HyperK (I-AniI), containing a silent G25G mutation to disrupt a cryptic splice site together with F80K and L232K substitutions; the Y2 variant of I-AniI, that includes F13Y and S111Y substitutions [Takeuchi R, et al. (December 2008) Optimization of in vivo activity of a bifunctional homing endonuclease and maturase reverses evolutionary degradation. *Nucleic Acids Res*, 10.1093/nar/gkn1007]; and a catalytically inactive dead mutant of Y2 I-AniI nickase that includes an additional active-site Q171K substitution in addition to the nickase K227M substitution (see *Results*).